ELSEVIER

Solid State Ionics 110 (1998) 21–28

SOLID STATE IONICS

Transport properties of $LiMn_2O_4$ electrode materials for lithium-ion batteries

Jie Guan, Meilin Liu*

School of Materials Science and Engineering, Georgia Institute of Technology, Atlanta, GA 30332-0245, USA

Received 27 January 1998; accepted 9 February 1998

Abstract

Transport properties of $LiMn_2O_4$ prepared under different conditions are characterized using impedance spectroscopy and 4-probe DC techniques. Results indicate that $LiMn_2O_4$ is a mixed ionic–electronic conductor with lithium-ion transference number varying from about 0.67 to 0.92, depending on conditions of preparation. It is observed that $LiMn_2O_4$ powders synthesized at low temperatures exhibit higher total conductivities than those synthesized at high temperatures. Among the $LiMn_2O_4$ powders synthesized at high temperatures, the ones quenched in liquid nitrogen have lower activation energy than the ones cooled down slowly. Further, cycling of $Li \mid P(EO)_8LiCF_3SO_3 \mid Li_xMn_2O_4$ cells indicates that the $LiMn_2O_4$ powders synthesized at a low temperature exhibit much higher obtainable capacity than those synthesized at high temperatures under the same cycling conditions.

Keywords: Lithium manganese oxides; Electrodes; Lithium-ion batteries; Mixed conductors

1. Introduction

The demand for compact and high-energy density batteries increases continuously with miniaturization in microelectronics and advances in portable devices. Among various alternative power systems, lithium batteries offer the greatest promise for high energy and power density or portability. Recent studies on lithium-ion batteries indicate that the development of inexpensive and environment-friendly electrode materials with high capacity and adequate reversibility is critical to successful development of viable battery systems [1–4]. Although various positive electrode materials have been studied for lithium-ion batteries, $LiMn_2O_4$ is more attractive than other materials (such as $LiCoO_2$ and $LiNiO_2$) because of its low cost and environmental compatibility [5–10].

Since the electrochemical performance of electrodes is greatly influenced by the crystal structures and microstructures of the electrode materials, which are determined by the preparation conditions, several synthesis approaches for lithium manganese oxides have been investigated, such as the Pechini process [11,12], glycine nitrate process [11], solid state reaction [13], sol–gel [14], and acetate approaches [15]. In particular, attention has been focused on synthesis of fine powders for positive electrodes at low temperatures to achieve high capacity and reversibility [16]. The transport properties of $LiMn_2O_4$, however, have not been well studied although sufficient lithium-ion and electron conduc-

*Corresponding author: Tel.: +1 404 894 6114; fax: +1 404 894 9140; e-mail: meilin.liu@mse.gatech.edu

0167-2738/98/$19.00
PII: S0167-2738(98)00096-4

tivities are essential to the performance of a $LiMn_2O_4$ electrode. There are also some discrepancies in the literature on electrical properties of $LiMn_2O_4$. For example, Pistoia et al. [17] indicated that $LiMn_2O_4$ was a hopping semiconductor with conductivity of about 2×10^{-6} Ω^{-1} cm^{-1} while Chen and Schoonman [18] reported that the total conductivity was closed to 10^{-4} Ω^{-1} cm^{-1} at room temperature determined from impedance measurements on pellets sintered at 1100 and 1200°C. Feltz et al. [19] reported that the electrical conductivity of $LiMn_2O_4$ was about 2.3×10^{-4} Ω^{-1} cm^{-1} at 20°C with an activation energy of 0.346 eV determined from DC measurements on pellets sintered at 1000°C followed by annealing and quenching. In this paper, transport properties of $LiMn_2O_4$ prepared under different conditions are characterized in a solid-state cell using impedance spectroscopy and 4-probe techniques. The electrochemical properties of the prepared $LiMn_2O_4$ are correlated with the crystal and defect structures and further with the synthesis and processing conditions.

2. Experimental

2.1. Sample preparation

$LiMn_2O_4$ powders were prepared from acetates using either xerogel method [20] or solid state reaction. In the xerogel approach, manganese and lithium acetates (Adrich) with a desired stoichiometric ratio were dissolved in a minimum amount of methanol, to which a proper amount of 1 M aqueous citric acid solution was added while the solution was stirred. Homogenous precipitates (manganese citrates) were formed and finely dispersed in the solution medium due to their low solubility. Solvents were evaporated slowly until xerogel type solid phases were obtained, which were then fired at 300°C (XE300N) and 800°C (XE800N) for 15 h. In the solid state reaction approach, Li_2CO_3 (Adrich) and λ-MnO_2 (Chemetals) powders were ball-milled in a desired stoichiometric ratio. The resulted mixtures were calcined at 800°C for 15 h and then were cooled down to ambient temperature by natural cooling ($\approx$6°C min^{-1}, SS800N), slow cooling (0.5°C min^{-1}, SS800A), and quenching in liquid nitrogen (SS800Q).

The obtained powders were mixed with 5 wt.% polyvinylidene fluoride (PVDF, Adrich) and ball-milled in ethanol for 20 h. The resulted mixtures were then dried and pressed into pellets (1.9 cm in diameter) under a pressure of 375 MPa. Sample XE800S was prepared by pressing XE800N powders under the same pressure and then fired at 800°C for 15 h. The thickness of the tested samples varied from 2.25 to 2.55 mm.

Polyethylene oxide (PEO)-based electrolyte was prepared by dissolving lithium triflate (Adrich) and PEO (M_w = 900 000, Adrich) in acetonitrile. The ratio of PEO to lithium triflate was such to form an electrolyte with composition of $P(EO)_8LiCF_3SO_3$. The composite positive electrode for the cycling study was prepared by adding $LiMn_2O_4$ and graphite powders (Alfa) to $P(EO)_8LiCF_3SO_3$ solution in acetonitrile to form a $LiMn_2O_4$ slurry. The weight ratio of $LiMn_2O_4$ to graphite and to $P(EO)_8LiCF_3SO_3$ was 40:10:50. Electrolyte and composite positive electrode films were prepared by casting the $P(EO)_8LiCF_3SO_3$ solution in acetonitrile and the $LiMn_2O_4$ slurry into glass rings on PARA films, respectively.

2.2. Microscopic characterization

The obtained $LiMn_2O_4$ powders were examined using X-ray diffractometer (XRD; Phillips PW1800, Cu Kα radiation). The lattice constant was calculated with an uncertainty of $\pm$0.002 Å using (440) peak in the cubic lattice. The particle size and morphology was analyzed using a scanning electron microscope (SEM; Hitachi S-800). The relative densities of the pellets pressed with PVDF binder were estimated to be about 67% from the pellet weight, volume, and the densities of PVDF and $LiMn_2O_4$. The relative density of the sintered pellet (XE800S) was determined to be about 81 vol.% based on stereological analysis of SEM micrographs [21].

2.3. Four-probe measurements

The cell for 4-probe measurement [22] consists of two lithium foils (Lithco), two pieces of $P(EO)_8LiCF_3SO_3$ films, and one $LiMn_2O_4$ pellet as

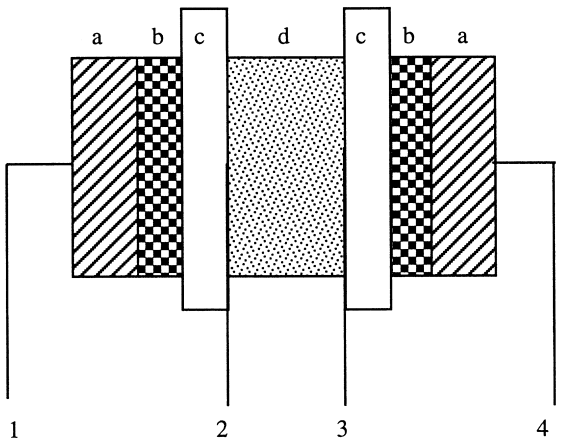

(1) Working Electrode
(2) Sensing Electrode
(3) Reference Electrode
(4) Counter Electrode
(a) Stainless Steel
(b) Lithium Metal
(c) $P(EO)_8LiCF_3SO_3$
(d) $LiMn_2O_4$

Fig. 1. A schematic diagram of a cell for 4-probe measurement.

schematically shown in Fig. 1. Two Ag wires were positioned as sensing and reference electrodes between $LiMn_2O_4$ pellet and the adjacent PEO-based electrolyte films. All air-sensitive materials were handled in an argon-filled glove box (VAC, DRI-LAB).

The impedance spectra of $LiMn_2O_4$ pellets were acquired from probe 2 and 3 (as shown in Fig. 1) using an EG&G impedance system (EG&G 273A and Lock-in Amplifier 5210), from which the total resistance (R_t) of the $LiMn_2O_4$ pellet can be directly read from the intercept of the impedance loop at low frequencies. The resistance to the motion of lithium ions was determined from DC measurements. When a constant DC current (I_a) was applied through the probe 1 and 4, both electronic and ionic species will respond initially. In a steady state, however, the current flow would be due merely to the motion of lithium ions since the electronic transport will be blocked by the lithium-ion conductive $P(EO)_8LiCF_3SO_3$ films. The steady-state voltages (V_{ss}) across a $LiMn_2O_4$ pellet can be read from probe 2 and 3. The lithium-ion resistance (R_{Li}) is given by

$$R_{Li} = \frac{V_{ss}}{I_a}, \tag{1}$$

and the lithium-ion transference number can then be approximated by

$$t_{Li} = \frac{R_t}{R_{Li}}. \tag{2}$$

Thus, the total and lithium-ion conductivities (σ_t and σ_{Li}) can be obtained from R_t, R_{Li}, and the dimen-

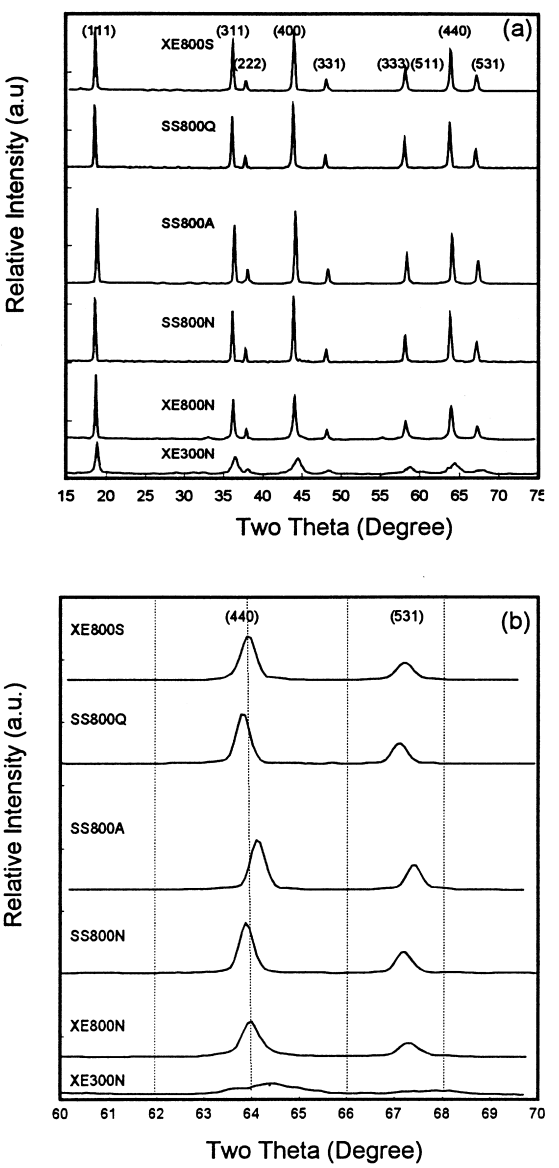

Fig. 2. X-ray diffraction patterns for $LiMn_2O_4$ powders prepared under different conditions: (a) the spinel phases and (b) peak shift due to different synthesis conditions.

sions of the sample, while the electronic conductivities are estimated from

$$\sigma_e = \sigma_t(1 - t_{Li}). \quad (3)$$

2.4. Cell assembly and cycling

Cycling behavior of $LiMn_2O_4$ powders was also studied using solid-state cells. The composite electrode film was cut, weighed, and used as positive electrode while lithium metal was used as negative electrode. The positive electrode film, $P(EO)_8LiCF_3SO_3$ electrolyte film, and negative electrode were laminated between two stainless steel blocks to form a cell for testing. Cells were cycled in an oven kept at 90°C at a rate of 0.35 mA cm^{-2} with a cutoff voltage of 2 V for discharge and 5 V for charge.

3. Results and discussion

3.1. Crystal structure and microstructure

Shown in Fig. 2(a) are the XRD patterns of the six samples prepared under different conditions (Table 1). Although they all have spinel structure, the diffraction peaks do shift slightly as can be seen in Fig. 2(b). The preparation conditions and lattice constants of $LiMn_2O_4$ powders are summarized in Table 1. Clearly, the powder prepared at a low temperature (XE300N) has a smaller lattice constant than those prepared at high temperatures. The quenched sample (SS800Q) has the largest lattice constant. The SEM micrographs seen in Fig. 3 clearly show that the average particle size of XE300N is much smaller than those of XE800N and SS800N.

Table 1
Preparation conditions and measured lattice constants of $LiMn_2O_4$ powders

Sample	Synthesis method	Synthesis conditions		Lattice constant (Å)
		Fired for 15 h at	Cooling rate	
XE300N	Xerogel	300°C	≈6°C min^{-1}	8.179
XE800N		800°C	≈6°C min^{-1}	8.228
XE800S		800°C	≈6°C min^{-1}	8.230
SS800A	Solid state reaction	800°C	0.5°C min^{-1}	8.221
SS800N		800°C	≈6°C min^{-1}	8.231
SS800Q		800°C	quenched in LN	8.241

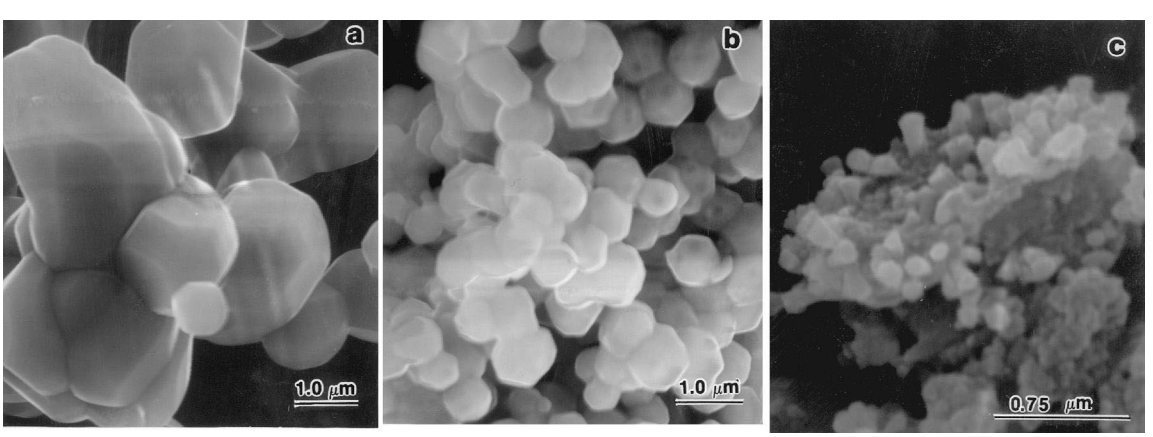

Fig. 3. SEM micrographs for (a) SS800N, (b) XE800N, and (c) XE300N $LiMn_2O_4$ powders.

3.2. Transport properties

Shown in Fig. 4 are the typical impedance spectra, voltage–time curves, and current–voltage characteristics of a $LiMn_2O_4$ pellet (XE300N) as measured using a 4-probe cell. Lithium-ion resistance (R_{Li}), total resistance (R_t), lithium-ion transference number (t_{Li}), and electronic conductivity can be readily determined from these data. Shown in Fig. 5 are the lithium-ion transference numbers of different samples measured in the temperature range of 30 to

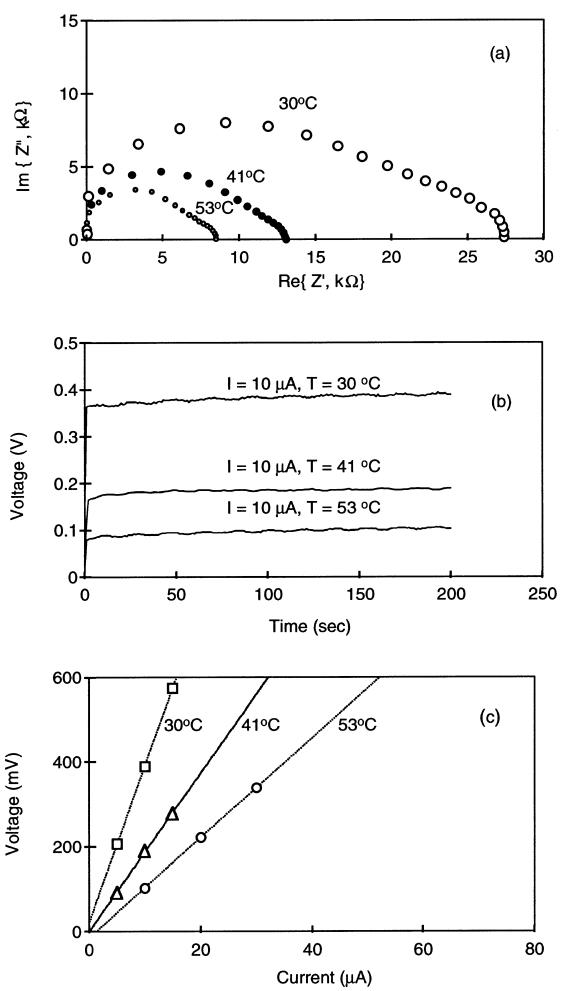

Fig. 4. Typical (a) impedance spectra, (b) voltage between probe 2 and 3 as a function of time when a constant current was applied between probe 1 and 4, and (c) *V–I* curves for a pellet (thickness = 2.25 mm and diameter = 19 mm) formed by pressing XE300N powder with PVDF.

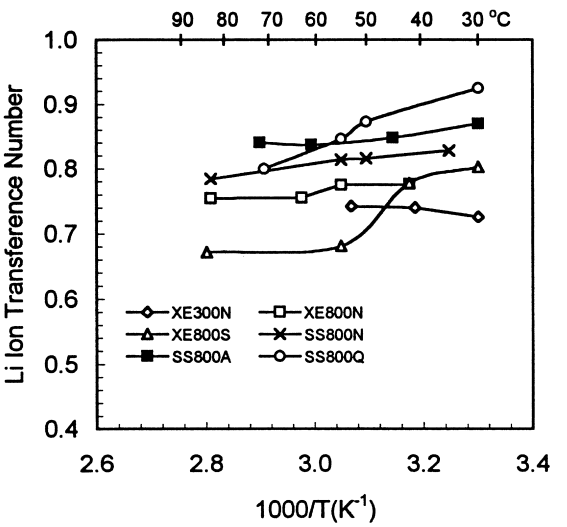

Fig. 5. Lithium-ion transference numbers of various samples measured at different temperatures.

84°C, suggesting $LiMn_2O_4$ be a mixed ionic–electronic conductor with dominating lithium-ion conduction. Thus, an electronically conductive phase, such as carbon, may be necessary in order to form a composite electrode with adequate electronic conductivity [6]. As shown in Fig. 6(a), the total conductivities of sintered pellets ($\approx 5.76\times10^{-5}$ Ω^{-1} cm^{-1} at 30°C) without PVDF binder are much higher than those of pellets pressed with PVDF binder. This is expected since sintered pellet has higher density. Among the five samples containing PVDF as binder, XE300N (prepared at a low temperature) has the highest total conductivity ($\approx 2.95\times10^{-6}$ Ω^{-1} cm^{-1} at 30°C) while SS800A has the lowest total conductivity ($\approx 9.9\times10^{-7}$ Ω^{-1} cm^{-1} at 30°C). The powder prepared at a low temperature (such as XE300N) tends to have smaller particle size, more defects, and higher conductivity than the powders prepared at higher temperatures and cooled slowly (such as SS800A). However, the sample prepared at 800°C and quenched in liquid nitrogen showed a small activation energy ($\approx$0.245 eV) for total conductivity, as can be seen from the slope of SS800Q in the Arrhenius plot (Fig. 6(a)).

The dependence of lithium-ion conductivity on temperature (Fig. 6(b)) is very similar to that of total conductivity (Fig. 6(a)) because of the predominant lithium-ion conduction. The lowest activation energy

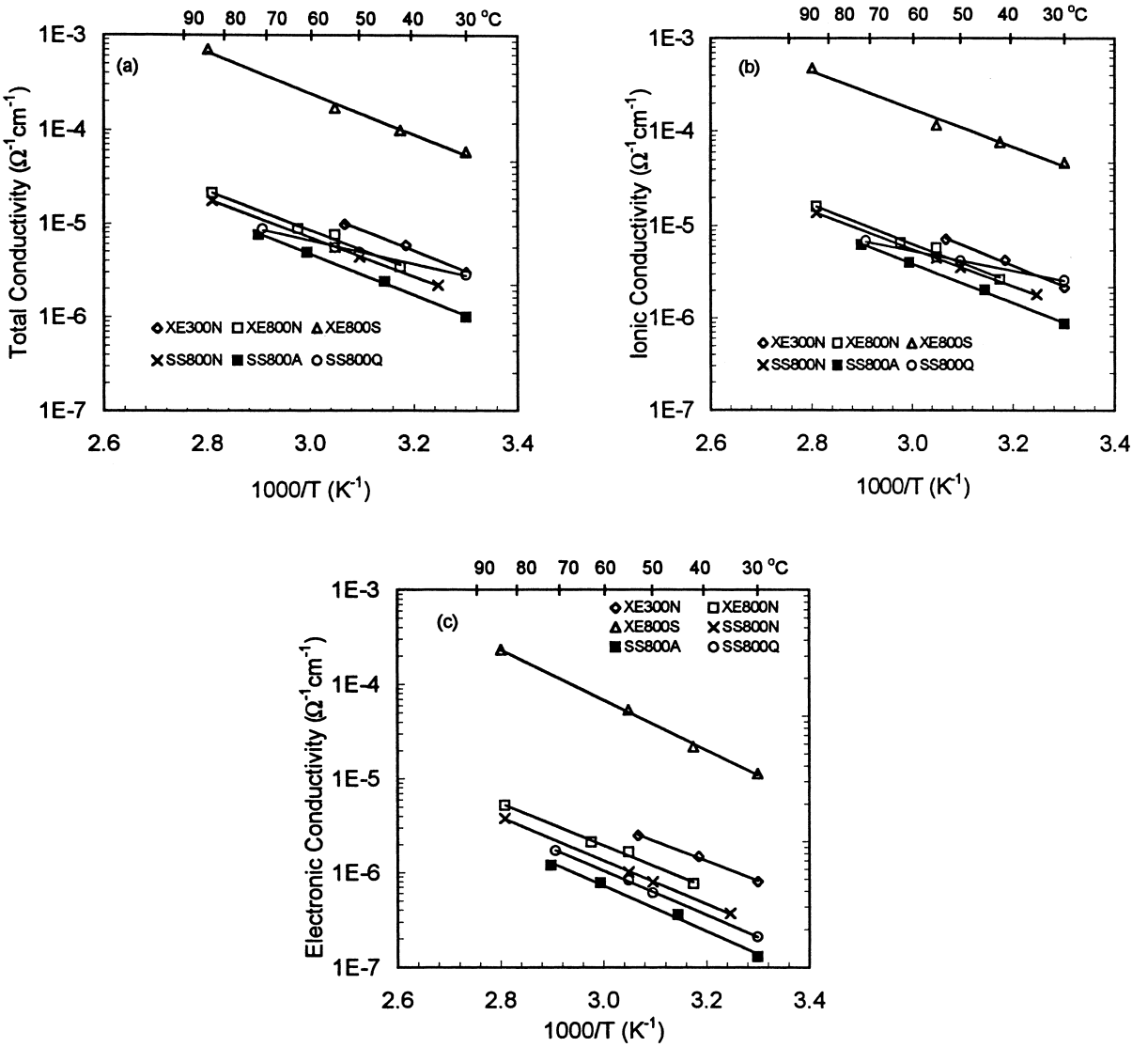

Fig. 6. Temperature dependence of (a) total, (b) ionic, and (c) electronic conductivities of samples prepared under different conditions.

($E_a \approx 0.216$ eV) for lithium-ion conductivity was observed in the quenched sample with the largest lattice constant; while the activation energies for other samples varied from 0.4 to 0.45 eV. In general, the more open the $LiMn_2O_4$ spinel structure, the easier the motion of lithium cations since the electrostatic and bonding forces would be weakened by the enlarged distance between lithium cations and oxygen anions [1].

The sample labeled with XE300N has the highest electronic conductivity among the samples with PVDF binder (Fig. 6(c)) as a result of its smallest lattice constant. Since the electronic conduction in the $LiMn_2O_4$ spinel is believed due to hopping electrons between mixed valence Mn [23], small lattice size implies more overlap in wave functions of neighboring Mn with different valence and, thus, enhances the electronic conductivity. The variation in interatomic distance which influences the overlap of the involved wave functions, may cause a metal–

semiconductor (insulator) transition in spinel structure. The critical cation–cation separation in the octahedral configuration of spinel lattice is given by [23]

$$R_c = 3.20 - 0.05m - 0.03(Z - Z_{Ti}) - 0.04S(S+1), \quad (4)$$

where m is the oxidation state of Mn ($+3.5$), Z is the atomic number of Mn, Z_{Ti} is the atomic number of Ti as a reference, and S is the effective spin for Mn^{3+}/Mn^{4+} given by

$$S = \frac{1}{2}\left(4 \times \frac{1}{2} + 3 \times \frac{1}{2}\right) = 1.75. \quad (5)$$

A critical value of 2.743 Å was calculated for $LiMn_2O_4$ spinel using Eq. (4), implying that $LiMn_2O_4$ would exhibit metallic characteristics due to significant overlap of the 3d electrons if the distance of Mn–Mn is less than 2.743 Å and otherwise, the material exhibits semiconductor characteristics. The actual Mn–Mn distances were calculated from

$$R_{Mn-Mn} = \frac{a\sqrt{2}}{4}, \quad (6)$$

using the lattice constant listed in Table 1. All the six samples had Mn–Mn separation (>2.90 Å) greater than the critical value, suggesting $LiMn_2O_4$ remain as a semiconductor, unlike LiV_2O_4 which is a metallic conductor [23,24].

3.3. Electrochemical properties

Shown in Fig. 7 are some typical charge and discharge curves for solid-state cells using PEO-based electrolyte, lithium metal negative electrode, and $LiMn_2O_4$ positive electrodes. Much higher capacity was obtained with a cell using XE300N powder in comparison to a cell using SS800N powder. The smaller the particle size, the shorter the diffusion path for lithium ions and the smaller the change in the volume to surface area of individual particles during charge/discharge cycling [1]. Thus, XE300N powder with smaller particle size exhibited higher obtainable capacity than SS800N powder with larger particle size.

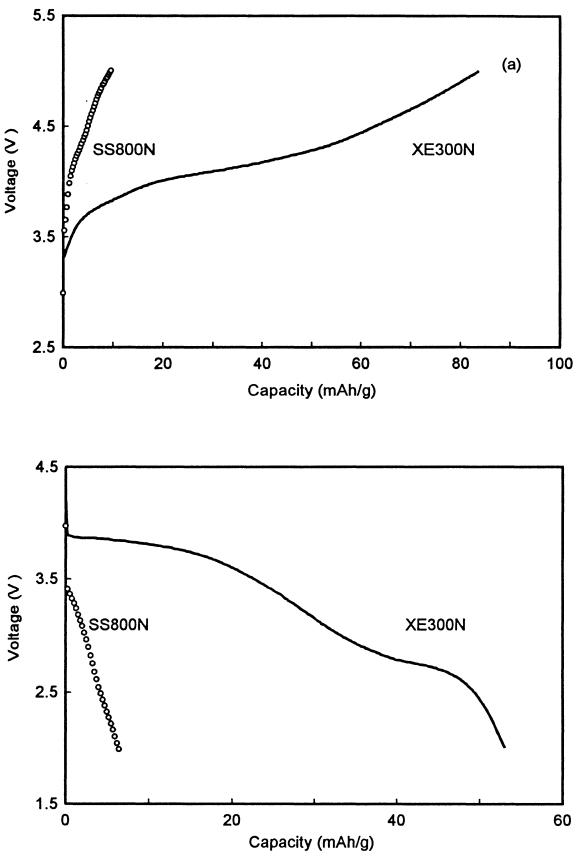

Fig. 7. (a) charge and (b) discharge curves of solid-state cells measured at 90°C using XE300N and SS800N powders as positive electrodes. The charge and discharge rates were 0.35 mA cm^{-2}.

4. Conclusions

Spinel $LiMn_2O_4$ is a mixed ionic–electronic conductor with predominant lithium-ion conduction ($t_{Li} > 0.6$) and the introduction of an electronically conductive phase to form a composite electrode is necessary in order to have adequate ambipolar conductivity for electrode functions. Results indicate that quenching $LiMn_2O_4$ powders from high temperature (800°C) to liquid nitrogen increases the lattice constant and reduces the activation energy for lithium-ion conduction. However, it appears that the $LiMn_2O_4$ powders synthesized at a low temperature exhibit high conductivity, which is primarily attributed to smaller particle size and more defects. In addition, the $LiMn_2O_4$ powder with smaller particle size exhibits higher obtainable capacity than the ones

with larger particle size under identical cycling conditions.

Acknowledgements

This work was supported by National Science Foundation under Award No. DMR-9357520 and NSF's support is gratefully acknowledged.

References

[1] J.B. Goodenough, Solid State Ionics 69 (1994) 184.
[2] J.B. Goodenough, A. Manthiram, B. Wnetrzewski, J. Power Sources 43–44 (1993) 269.
[3] A. Manthiram, JOM 3 (1997) 43.
[4] J.N. Reimers, E.W. Fuller, E. Rossen, J.R. Dahn, J. Electrochem. Soc. 140 (1993) 3396.
[5] M.M. Thackeray, W.I.F. David, P.G. Bruce, J.B. Goodenough, Mater. Res. Bull. 18 (1983) 461.
[6] J.M. Tarascon, D. Guyomard, Electrochim. Acta 38 (1993) 1221.
[7] S. Megahed, B. Scrosati, J. Power Sources 51 (1994) 79.
[8] R. Bittihn, R. Herr, D. Hoge, J. Power Sources 43–44 (1993) 223.
[9] T. Ohzuku, A. Ueda, Solid State Ionics 69 (1994) 201.
[10] M.M. Thackeray, J. Electrochem. Soc. 142 (1995) 2558.
[11] J. Guan, M. Liu, in: P.N. Kumta, G.S. Rohrer, U. Balachandran (Eds.), Role of Ceramics in Advanced Electrochemical Systems, Ceramic Trans. 65 (1996) 149.
[12] W. Liu, G.C. Farrington, F. Chaput, B. Dunn, J. Electrochem. Soc. 143 (1996) 879.
[13] A. Monchilov, V. Manev, A. Nassalevska, J. Power Sources 41 (1993) 305.
[14] S. Bach, M. Henry, N. Baffier, J. Livage, J. Solid State Chem. 88 (1990) 325.
[15] P. Barboux, J.M. Tarascon, F.K. Shokoohi, J. Solid State Chem. 94 (1991) 185.
[16] P. Barboux, F.K. Shokoohi, J.M. Tarascon, U.S. Patent 5 135 732.
[17] G. Pistoia, D. Zane, Y. Zhang, J. Electrochem. Soc. 142 (1995) 2551.
[18] L. Chen, Schoonman, Solid State Ionics 67 (1994) 17.
[19] J. Topher, A. Feltz, J. Alloys Comp. 202 (1993) 231.
[20] S.R. Sahaya Prabaharan, M. Siluvai Michael, T. Prem Kumar, A. Mani, K. Athinarayanaswamy, R. Gangadharan, J. Mater. Chem. 5 (1995) 1035.
[21] E.E. Underwood, Quantitative Microscopy, McGraw, New York, 1966.
[22] M. Liu, S.J. Visco, L.C. De Jonghe, Electrochim. Acta 38 (1993) 1289.
[23] J.B. Goodenough, Progr. Solid State Chem. 5 (1971) 145.
[24] L.A. De Picciotto, M.M. Thackeray, Solid State Ionics 28–30 (1988) 1364.